C h a p t e r 4

THERMAL BIOSWITCHES FOR MODULAR CONTROL OF PROTEIN DIMERIZATION

4.1: Introduction

The study and engineering of cellular function within the context of complex tissues and synthetic biomaterials necessitates the development of methods to enable external control of cellular signaling with high spatial and temporal specificity and deep tissue penetration[1]. Conditional protein-protein interactions (PPIs) are among the most widespread and versatile modalities employed by cells to regulate molecular signaling pathways[2]. Consequently, engineered PPIs have had an important role in studying the function of many proteins in the cell and the construction of synthetic cellular devices. In particular, widely used chemically-inducible dimerization domains such as FKBP/FRB[3] have enabled a vast array of applications ranging from the basic study of protein signaling[4] to the engineering of exogenously-gated chimeric antigen receptors for cellular immunotherapy[5]. Chemical dimerization is effective both in culture and in deep tissues based on the bioavailability of the chemical agent; however, this activity is poorly amenable to spatiotemporal regulation. In contrast, optically inducible dimerization domains such as Cry2/CIB1 offer exquisite spatial and temporal precision, enabling microscopic studies of processes such as the immune response[6] and cell motility[7], but are limited by the scattering of photons in deep tissue and other complex media.

Temperature offers an alternative mechanism for controlling biological signaling with several advantages over chemicals and light. Temperature can be applied to biological samples globally using simple heat sources or electromagnetic radiation, and can be applied locally deep within scattering media using technologies such as focused ultrasound, enabling spatiotemporal control with millimeter spatial resolution and temporal resolution on the order of seconds[1,8]. Previous work on thermal control of cellular signaling has focused on temperature-actuated transcription and translation, taking advantage of endogenous heat shock promoters[9,10], temperature-dependent RNA elements[11], or heterologously expressed protein-based transcriptional bioswitches[12]. In addition, temperature-sensitive variants of individual proteins have been used to study the function of these proteins in model systems[13,14]. While these pioneering approaches enable thermal control of specific aspects of cellular function, they lack the modularity of chemical and optical dimerizers.

Here we introduce a modular approach to controlling protein dimerization with temperature. Starting with a homodimeric temperature-dependent coiled-coil transcription factor from bacteria, we engineer a pair of heterodimeric protein association domains with sharp, tunable thermal unbinding. We demonstrate the ability of these "thermomers" to dynamically control protein localization in living mammalian cells. The resulting technology has the potential to provide versatile thermal control of protein-protein interactions in a variety of cell types, complementing the existing set of chemical and optical tools.

4.2: Results

As the starting point for our design of thermomers, we used the temperature-sensitive transcriptional repressor TlpA from *Salmonella typhimurium* due to its relatively simple architecture and well-characterized thermal behavior[15]. While no atomic-resolution structure of this protein exists, biochemical and bioinformatics studies have indicated that TlpA consists of an N-terminal DNA-binding domain and a C-terminal coiled-coil domain, the latter of which causes the protein to homodimerize in a temperature-dependent manner. As a dimer, TlpA binds to a cognate DNA operator sequence within its corresponding promoter and prevents transcription. The coiled-coil domain of TlpA undimerizes and uncoils above a temperature of ~42ºC, causing unbinding from the operator and allowing transcription to take place. This sharply cooperative transition happens over less than 3 ºC, as defined by 10% to 90% activation. We previously demonstrated that the thermal set-point of TlpA could be tuned through directed evolution without compromising cooperativity, and used its transcription factor activity to spatiotemporally control the function of engineered bacteria with ultrasound hyperthermia[12].

To turn TlpA into a modular protein-protein dimerization system, we first needed to convert it from a homodimer to a heterodimer. Most applications of inducible dimerization systems require the interacting modules to be heterodimeric to enforce selective binding between two desired molecular partners[16]. To redesign the wild type TlpA into a pair of heterodimeric coiled-coil species (**Fig. 4-1a**), we used rational mutagenesis guided by bioinformatic prediction of the TlpA dimerization domain. Coiled-coil domains typically consist of repetitive seven-amino acid residue sequences known as heptad repeats[17]. We used a

published annotation of the TlpA sequence[18], cross-referenced against a computational annotation from the COILS[19] prediction server, to establish the register of heptad repeats within the TlpA primary sequence. We then introduced charge-complementary pairs of residues[20] predicted either at conventional g-to-e' contacts or at alternative g-to-d' interfaces to disfavor homodimerization and favor heterodimerization (**Fig. 4-1, b-c**). The latter architecture occurs when large ionic sidechains at the core peripherally expose their charged termini as has been described for the Fos-Jun coiled coil interaction[21]. To maintain the highly switch-like thermal dissociation behavior of TlpA, we reasoned that the least perturbative positions for mutagenesis would be at existing interfacial ionic interaction sites in the wild type protein, which are present due to the C_2 symmetry of the parallel coiled-coil structure. We mutagenized all such positions one by one, replacing cationic residues with glutamate and anionic side chains with arginine or lysine. We expressed the resulting coiled-coil domains in *E. coli*, purified the proteins via affinity chromatography, and assayed their helical content over a relevant thermal range via circular dichroism spectroscopy (**Supplementary Fig. 4-S1**). From this initial screen we obtained a pair of charge-complemented mutants, dubbed TlpA-G_1A (E180R) and TlpA-G_1B (R179E), that demonstrated a sharp, sigmoidal switching profile with a notable upshift in threshold for an equimolar mixture of the mutant pair relative to pure solutions of either species (**Fig. 4-1d**).

To validate the *in vivo* functionality of the TlpA-G_1A and G_1B mutants, we utilized the ability of TlpA to modulate the expression of a fluorescent reporter gene in *E. coli*[12]. We constructed a temperature-inducible circuit containing two separate copies of the TlpA gene, with a TlpA operator upstream of a green fluorescent protein (GFP) and a red fluorescent protein (RFP).

To compare the repression efficiency of the G_1A/G_1A and G_1B/G_1B homodimers to that of the G_1A/G_1B heterodimer, we generated circuit variants containing two copies of TlpA-G_1A, two copies of TlpA-G_1B, or one copy of each TlpA strand (**Fig. 4-2a**). The thermal gene expression profiles of GFP showed all three circuits to produce a highly switch-like cooperative activation. However, the two homodimeric constructs had a clear downshift in their transition temperature compared to the heterodimeric construct containing both TlpA variants (**Fig. 4-2b**), confirming a stabilized heterotypic-association between the two coiled-coil strands. The RFP output displayed similar activation profiles (**Supplementary Fig. 4-S2**). Swapping the positions of the two TlpA copies within the vector did not significantly influence the expression profile, controlling for inadvertent stoichiometric effects (**Supplementary Fig. 4-S3**).

While the performance of the first-generation heterodimers was encouraging, we noted that the G_1A/G_1A and G_1B/G_1B circuit constructs still demonstrated an activation setpoint above 37 °C, indicating that the mutants retained the ability to homodimerize under typical mammalian homeostatic conditions. We therefore used our thermal GFP expression assay to evaluate a subset of additional rational mutant pairs selected from our original panel (**Supplementary Fig. 4-S4**), and chose the two best-performing pairs of substitutions from this subset to combine with TlpA G_1A and TlpA G_1B in all possible permutations. This resulted in the second-generation coiled-coil pairs dubbed TlpA $G_{2\text{-}1} – G_{2\text{-}4}$, each comprising a G_2A_n and a G_2B_n monomer (**Supplementary Table 4-T1**). In our bacterial bioswitch assay, all the heterodimeric circuits combining G_2A_n with its complementary G_2B_n displayed switch-like activation of reporter fluorescence (**Fig. 4-2c, Supplementary Fig. 4-S5**). In

contrast, the homodimeric constructs containing two copies of G_2A_n or G_2B_n were unable to propagate in a stable manner, consistently displaying deletions in the TlpA promoter or the fluorescent reporter gene, even when grown at 30 °C in recombination-deficient *E. coli*. We interpreted this as evidence that the second-generation variants are unable to form homodimeric interactions at the concentrations defined by our circuits, resulting in constitutive expression from the TlpA promoter and a strong metabolic burden to the host cell[22,23].

For additional confirmation of the dimerization preference of our engineered coiled-coils, we designed a biochemical assay based on covalent crosslinking and size-based gel separation. TlpA dimers can be crosslinked via $CuCl_2$-catalyzed oxidation of the protein's single cysteine residue[24]. To distinguish hetero- from homodimerization, we truncated one of the two TlpA sequences by removing its DNA binding domain, thereby altering its electrophoretic mobility on a polyacrylamide gel without perturbing its ability to dimerize (**Fig. 4-3a**). HA tags were added at the C-termini of both proteins to facilitate specific detection via Western blotting. We expressed the resulting pairs of truncated and full-length TlpA variants in *E. coli.* To validate this assay, we expressed a pair of wild-type TlpA coils and crosslinked them at 37 °C, after a thermal elevation to 45 °C, and after return to 37 °C. Three bands corresponding to the expected mixture of the two types of homodimers and one type of heterodimer were visible after crosslinking at 37 ºC, while crosslinking at the higher temperature resulted in the preponderance of monomers, which could be re-annealed by bringing the temperature back down to 37 ºC (**Fig. 4-3b**).

Substituting the wild type coiled-coils with our first-generation hetrodimerizing mutants resulted in preferential accumulation of the TlpA heterodimer at 37 °C (**Fig. 4-3c**). Constructs containing the second-generation variants demonstrated further reduction in the intensity of the homodimer bands in favor of the intermediate molecular weight heterodimer, with TlpA $G_{2\text{-}3}$ demonstrating the strongest heterodimeric enrichment. (**Fig. 4-3c, Supplementary Fig. 4-S6**). The first- and second-generation heterodimers both showed reversible dissociation at 45ºC (**Fig. 4-3d**). On the basis of these results, the TlpA $G_{2\text{-}3}$ pair was chosen as the thermomer construct for further experiments.

After validating our engineered heterodimeric TlpA thermomers, we set out to demonstrate their ability to be fused with other proteins and confer controlled protein-protein association in mammalian cells. We designed a construct wherein one TlpA-$G_{2\text{-}3}$ strand was N-terminally fused with the palmitoylation sequence of GAP43, thereby compartmentalizing it to the plasma membrane. The complementary strand was fused at the C-terminus to mScarlet-I (**Fig. 4-4a**), an RFP chosen for its robust fluorescence at elevated temperature (**Supplementary Fig. 4-S7**). To make this system compatible with mammalian homeostatic conditions, we combined the TlpA-$G_{2\text{-}3}$ heterodimerizing mutations with three previously described amino acid substitutions that lower the coiled-coil dissociation temperature to approximately 39 ºC[12].

Using live cell confocal microscopy of transiently transfected K562 cells, at physiological temperature we observed strong localization of red fluorescence to the plasma membrane (**Fig. 4-4b** and **Supplementary Fig. 4-S8**) and also to the Golgi apparatus (**Supplementary**

Fig. 4-S9). Increasing the cells' temperature using resistive heating above a threshold of 40 °C resulted in the redistribution of membrane fluorescence into the cytosol. As a control for non-specific thermal dissociation, cells in which the RFP was directly palmitoylated showed no redistribution of membrane fluorescence within this temperature range (**Fig. 4-4c**, **4-4d**, and **Supplementary Fig. 4-S10**). This confirms that RFP dissociation from the membrane is driven by a TlpA-mediated binding transition rather than disruption of membrane integrity.

To enable the use of the thermomer system with viral gene delivery and genomic integration, we generated a nonhomologous variant of the TlpA G_2A_3 strand (nhTlpA G_2A_3) in which all degenerate codons were mutagenized to synonymous triplets with minimal identity to the original sequence. This mutagenesis helps avoid template switching-mediated recombination during viral delivery of high-homology constructs[25]. The resulting open reading frame had 57.48% sequence identity to the parent sequence, with no more than 5 consecutive homologous nucleotides. Lentiviral delivery of a construct containing palmitoylated nhTlpA G_2A_3 and mScarlet-fused TlpA G_2B_3 resulted in robust temperature-induced dissociation of red fluorescence from the plasma membrane, similar to results from transient transfection (**Supplementary Fig. 4-S11**).

We used this virally-engineered K562 cell line to quantify the co-localization of RFP fluorescence intensity with signal from the plasma membrane as delineated by CellBrite Fix 488 staining (**Fig. 4-4e**). Cells with thermomer-mediated RFP targeting to the membrane demonstrated co-localization with the dye at physiological temperature, followed by loss of pixel correlation above 40 ºC (**Fig. 4-4f**). In contrast, control cells with directly palmitoylated

RFP demonstrate robust co-localization with the membrane stain throughout the temperature range tested, while free cytoplasmic RFP showed no correlation with the CellBrite dye (**Fig. 4-4f**). We also used the TlpA reporter cell line to evaluate the reversibility of TlpA-mediated membrane localization after heating. Membrane localization was released by a 5-minute incubation at 42 ºC. Upon cooling back to 37 °C, TlpA re-partitioned to the plasma membrane, indicating reversibility, albeit with slower kinetics than observed for dissociation (**Fig. 4-4g** and **Supplementary Fig. 4-S12 and 4-S13**).

4.3: Discussion

Our results establish heterodimeric TlpA coils as modular, tunable thermomers capable of conferring temperature-controlled protein-protein association and localization to genetically fused proteins. This technology complements the large existing repertoire of chemical and optical dimerizers used to control a wide range of protein and cellular functions[26]. The thermomer constructs also expand upon our previous work on temperature-stimulated transcriptional control[12] by enabling thermal actuation in arbitrary cell types and drastically increasing the kinetics of activation relative to that of gene expression. We anticipate that as external control of protein signaling becomes needed for more complex settings, such as cellular therapy[27] and engineered living materials[28], this will provide a role for temperature-based control modalities that offer spatiotemporal specificity and penetration depth beyond those afforded by systemic drug delivery or optical methods[1,8].

The simple architecture of the TlpA coiled-coil renders it an attractive domain for future work in controlling protein function. For example, conditionally dimeric coiled-coil fusions have previously been used to reconstitute and control a split mutant of RNAse T1[29] and to conditionally enact DNA binding by a bZIP domain upon photostimulation[30]. More broadly, coiled-coils have seen a diverse array of applications in biomaterials, affinity purification, assembly of bispecific or high avidity antibodies, and reconstitution of various split proteins or dimerization-dependent protein complexes[31,32].

To maximize its versatility as a tool for biology and medicine, future work on TlpA-based thermomers is needed to optimize construct size, modularity, and kinetics. At 371 residues, TlpA is nearly four times larger than its drug-responsive counterpart FKBP, which may hinder applications in gene delivery where sequence compactness is of premium importance. Truncation and mutagenesis approaches may offer a strategy by which the size of the thermomer system could be minimized without sacrificing the desired sharp thermal switching response. In addition, elucidating the mechanism responsible for the unique thermal cooperativity of TlpA would assist in future rational engineering efforts to modify performance and generate novel, orthogonal thermomers. Additionally, a thorough characterization of potential genetic fusion sites and optimal linker sequences would facilitate the widespread use of TlpA as a thermal fusion tag. In this study, we demonstrated that TlpA retains a cooperative thermal transition as an intact protein, as an isolated coiled-coil domain, and as a system with distinct fusion sites at the N and C-termini. However, additional engineering may be needed to accommodate fusion partners of different sizes and valency. Finally, we note that while detection of TlpA-RFP delocalization kinetics from the

plasma membrane appeared to be limited by the timescale of temperature elevation and image acquisition of our apparatus (approximately 2 minutes), re-association in some cells was significantly slower. It would be useful to investigate the factors that influence re-association, including diffusion and potential low-affinity contacts between unpartnered TlpA strands, their homodimeric partners and other constituents of the cell. With further optimization, thermomers promise to provide a high degree of control over a wide range of cellular processes with the versatile application of thermal energy.

4.4: Acknowledgements

The authors thank Mohamad Abedi and Andres Collazo for helpful discussions. Microscopy was performed at the Biological Imaging Facility of the Beckman Institute at Caltech. This research was supported by the Defense Advanced Research Projects Agency (D14AP0050), the Sontag Foundation and the Army Institute for Collaborative Biotechnologies (W911NF-19-D-0001). D.I.P. was supported by the NIH fellowship for Predoctoral Training in Biology and Chemistry (T32GM007616).

4.5: References

(1) Piraner, D. I.; Farhadi, A.; Davis, H. C.; Wu, D.; Maresca, D.; Szablowski, J. O.; Shapiro, M. G. Going Deeper: Biomolecular Tools for Acoustic and Magnetic Imaging and Control of Cellular Function. *Biochemistry* **2017**, *56* (39). https://doi.org/10.1021/acs.biochem.7b00443.

(2) Berggård, T.; Linse, S.; James, P. Methods for the Detection and Analysis of Protein – Protein Interactions. **2007**, 2833–2842. https://doi.org/10.1002/pmic.200700131.

(3) Spencer, D. M.; Wandless, T. J.; Schreiber, S. L.; Crabtree, G. R. Controlling Signal Transduction with Synthetic Ligands. *Science (80-.).* **1993**, *262* (5136), 1019–1024.

(4) Muthuswamy, S. K.; Gilman, M.; Brugge, J. S. Controlled Dimerization of ErbB Receptors Provides Evidence for Differential Signaling by Homo- and Heterodimers. *Mol. Cell. Biol.* **1999**, *19* (10), 6845–6857.

(5) Wu, C.-Y.; Roybal, K. T.; Puchner, E. M.; Onuffer, J.; Lim, W. A. Remote Control of Therapeutic T Cells through a Small Molecule-Gated Chimeric Receptor. *Science (80-.).* **2015**, *350* (6258). https://doi.org/10.1126/science.aab4077.

(6) Moser, B. A.; Esser-Kahn, A. P. A Photoactivatable Innate Immune Receptor for Optogenetic Inflammation. *ACS Chem. Biol.* **2017**, *12* (2), 347–350. https://doi.org/10.1021/acschembio.6b01012.

(7) Bugaj, L. J.; Choksi, A. T.; Mesuda, C. K.; Kane, R. S.; Schaffer, D. V. Optogenetic Protein Clustering and Signaling Activation in Mammalian Cells. **2013**, *10* (3). https://doi.org/10.1038/nmeth.2360.

(8) Maresca, D.; Lakshmanan, A.; Abedi, M.; Bar-Zion, A.; Farhadi, A.; Lu, G. J.; Szablowski, J. O.; Wu, D.; Yoo, S.; Shapiro, M. G. Biomolecular Ultrasound and Sonogenetics. *Annu. Rev. Chem. Biomol. Eng.* **2018**, *9*, 229–252. https://doi.org/10.1146/annurev-chembioeng-060817-084034.

(9) Guilhon, E.; Voisin, P.; de Zwart, J. a; Quesson, B.; Salomir, R.; Maurange, C.; Bouchaud, V.; Smirnov, P.; de Verneuil, H.; Vekris, a; et al. Spatial and Temporal Control of Transgene Expression in Vivo Using a Heat-Sensitive Promoter and MRI-Guided Focused Ultrasound. *J. Gene Med.* **2003**, *5* (4), 333–342. https://doi.org/10.1002/jgm.345.

(10) Liu, R. Y.; Corry, P. M.; Lee, Y. J. Regulation of Chemical Stress-Induced Hsp70 Gene Expression in Murine L929 Cells. *J. Cell Sci.* **1994**, *107*, 2209–2214.

(11) Krajewski, S. S.; Narberhaus, F. Temperature-Driven Differential Gene Expression by RNA Thermosensors. *Biochim. Biophys. Acta - Gene Regul. Mech.* **2014**, *1839* (10), 978–988. https://doi.org/10.1016/j.bbagrm.2014.03.006.

(12) Piraner, D. I.; Abedi, M. H.; Moser, B. A.; Lee-Gosselin, A.; Shapiro, M. G. Tunable Thermal Bioswitches for in Vivo Control of Microbial Therapeutics. *Nat. Chem. Biol.* **2017**, *13* (1), 75–80. https://doi.org/10.1038/nchembio.2233.

(13) Royal, D. C.; Bianchi, L.; Royal, M. A.; Lizzio, M.; Mukherjee, G.; Nunez, Y. O.; Driscoll, M. Temperature-Sensitive Mutant of the Caenorhabditis Elegans Neurotoxic MEC-4(d) DEG/ENaC Channel Identifies a Site Required for Trafficking or Surface Maintenance. *J. Biol. Chem.* **2005**, *280* (51), 41976–41986. https://doi.org/10.1074/jbc.M510732200.

(14) Cox, V. T.; Baylies, M. K. Specification of Individual Slouch Muscle Progenitors in Drosophila Requires Sequential Wingless Signaling. *Development* **2005**, *132*, 713–724. https://doi.org/10.1242/dev.01610.

(15) Hurme, R.; Berndt, K. D.; Normark, S. J.; Rhen, M. A Proteinaceous Gene Regulatory Thermometer in Salmonella. *Cell* **1997**, *90* (1), 55–64.

(16) Stanton, B. Z.; Chory, E. J.; Crabtree, G. R. Chemically Induced Proximity in Biology and Medicine. *Science (80-.).* **2018**, *359* (6380), 1–9. https://doi.org/10.1126/science.aao5902.

(17) Mason, J. M.; Arndt, K. M. Coiled Coil Domains: Stability, Specificity, and Biological Implications. *Chembiochem* **2004**, *5* (2), 170–176. https://doi.org/10.1002/cbic.200300781.

(18) Koski, P.; Saarilahti, H.; Sukupolvi, S.; Taira, S.; Riikonen, P.; Osterlund, K.; Hurme, R.; Rhen, M. A New Alpha-Helical Coiled Coil Protein Encoded by the Salmonella Typhimurium Virulence Plasmid. *J. Biol. Chem.* **1992**, *267* (17), 12258–12265.

(19) Lupas, a; Van Dyke, M.; Stock, J. Predicting Coiled Coils from Protein Sequences. *Science (80-.).* **1991**, *252* (5009), 1162–1164. https://doi.org/10.1126/science.252.5009.1162.

(20) Tripet, B.; Yu, L.; Bautista, D. L.; Wong, W. Y.; Irvin, R. T.; Hodges, R. S. Engineering a de Novo-Designed Coiled-Coil Heterodimerization Domain off the Rapid Detection, Purification and Characterization of Recombinantly Expressed Peptides and Proteins. *Protein Eng.* **1996**, *9* (11), 1029–1042. https://doi.org/10.1093/protein/9.11.1029.

(21) Azuma, Y.; Ku, T.; Yasunaga, J.; Imanishi, M.; Tanaka, G.; Nakase, I.; Maruno, T.; Kobayashi, Y.; Arndt, K. M.; Matsuoka, M.; et al. Controlling Leucine-Zipper Partner Recognition in Cells through Modification of a–g Interactions. *Chem Commun* **2014**, *50* (48), 6364–6367. https://doi.org/10.1039/c4cc00555d.

(22) Kawe, M.; Horn, U.; Plückthun, A. Facile Promoter Deletion in Escherichia Coli in Response to Leaky Expression of Very Robust and Benign Proteins from Common Expression Vectors. *Microb. Cell Fact.* **2009**, *8* (8), 1–8. https://doi.org/10.1186/1475-2859-8-8.

(23) Silva, F.; Queiroz, J. A.; Domingues, F. C. Evaluating Metabolic Stress and Plasmid Stability in Plasmid DNA Production by Escherichia Coli. *Biotechnol. Adv.* **2012**, *30* (3), 691–708. https://doi.org/10.1016/j.biotechadv.2011.12.005.

(24) Hurme, R.; Namork, E.; Nurmiaho-Lassila, E.-L.; Rhen, M. Intermediate Filament-like Network Formed in Vitro by a Bacterial Coiled Coil Protein. *J. Biol. Chem.* **1994**, *269* (14), 10675–10682.

(25) Delviks, K. A.; Pathak, V. K. Effect of Distance between Homologous Sequences and 3' Homology on the Frequency of Retroviral Reverse Transcriptase Template Switching. *J. Virol.* **1999**, *73* (10), 7923–7932.

(26) DeRose, R.; Miyamoto, T.; Inoue, T. Manipulating Signaling at Will: Chemically-Inducible Dimerization (CID) Techniques Resolve Problems in Cell Biology. *Pflügers Arch. - Eur. J. Physiol.* **2013**, *465* (3), 409–417. https://doi.org/10.1007/s00424-012-1208-6.

(27) Wu, C.-Y.; Rupp, L. J.; Roybal, K. T.; Lim, W. A. Synthetic Biology Approaches to Engineer T Cells. *Curr. Opin. Immunol.* **2015**, *35*, 123–130. https://doi.org/10.1016/j.coi.2015.06.015.

(28) Gilbert, C.; Ellis, T. Biological Engineered Living Materials – Growing Functional Materials with Genetically-Programmable Properties. *ACS Synth. Biol.* **2019**, *8* (1), 1–15. https://doi.org/10.1021/acssynbio.8b00423.

(29) Yuzawa, S.; Mizuno, T.; Tanaka, T. Activating an Enzyme by an Engineered Coiled Coil Switch. *Chem. Eur. J.* **2006**, *12*, 7345–7352. https://doi.org/10.1002/chem.200600007.

(30) Woolley, G. A.; Jaikaran, A. S. I.; Berezovski, M.; Calarco, J. P.; Krylov, S. N.; Smart, O. S.; Kumita, J. R. Reversible Photocontrol of DNA Binding by a Designed GCN4-BZIP Protein. *Biochemistry* **2006**, *45*, 6075–6084.

(31) Apostolovic, B.; Danial, M.; Klok, H.-A. Coiled Coils: Attractive Protein Folding Motifs for the Fabrication of Self-Assembled, Responsive and Bioactive Materials. *Chem. Soc. Rev.* **2010**, *39*, 3541–3575. https://doi.org/10.1039/b914339b.

(32) Muller, K. M.; Arndt, K. M.; Alber, T. Protein Fusions to Coiled-Coil Domains. In *Methods in Enzymology*; 2000; Vol. 328, pp 261–282. https://doi.org/10.1016/S0076-6879(00)28402-4.

4.6: Main Figures

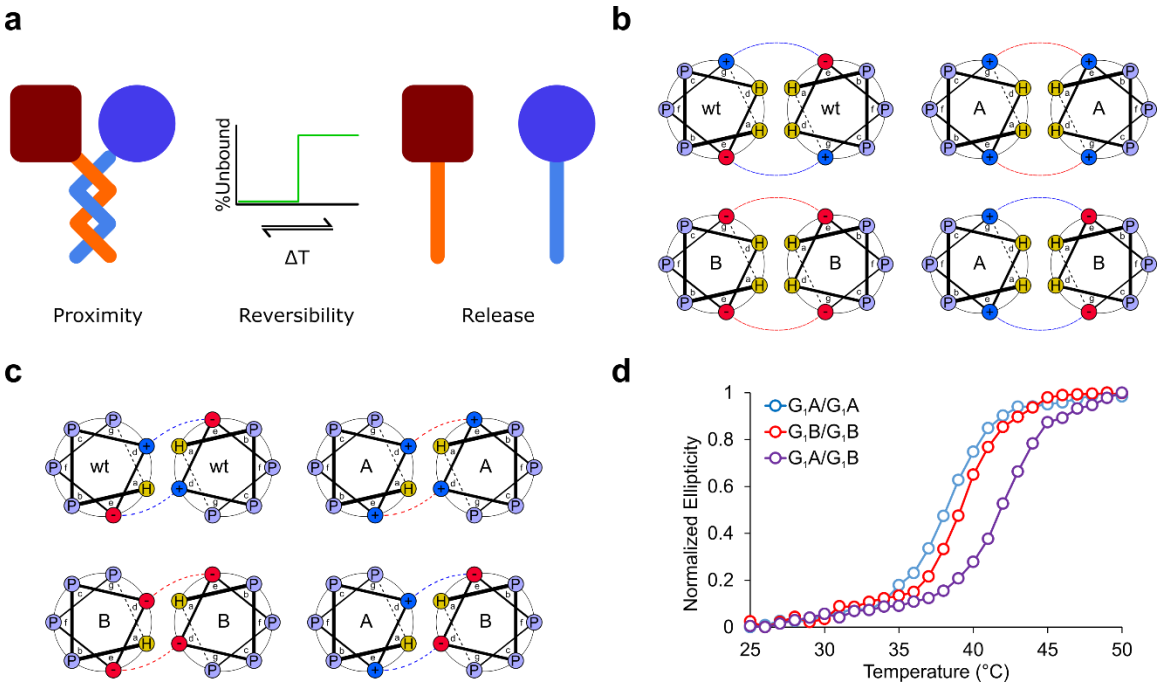

Figure 4-1: Engineering heterodimeric TlpA variants via charge-charge complementation. a) Illustration of TlpA-based thermomer system. Heterodimeric coiled-coil domains enable reversible association and dissociation of fusion partners as a sharp function of temperature. **b**) Diagram of heterodimeric coiled-coil design based on the introduction or modification of electrostatic contacts at the e-to-g' interface between adjacent α-helices. **c**) Diagram of predicted electrostatic contacts along the TlpA interface occurring in a nonconventional e-to-d' configuration. **d**) Normalized ellipticity of purified TlpA coiled-coil domain variants in isolation or as an equimolar mixture, measured at the 222 nm peak for α-helical spectra as a function of temperature. Data shown normalized from 0 to 1 on a per-sample basis.

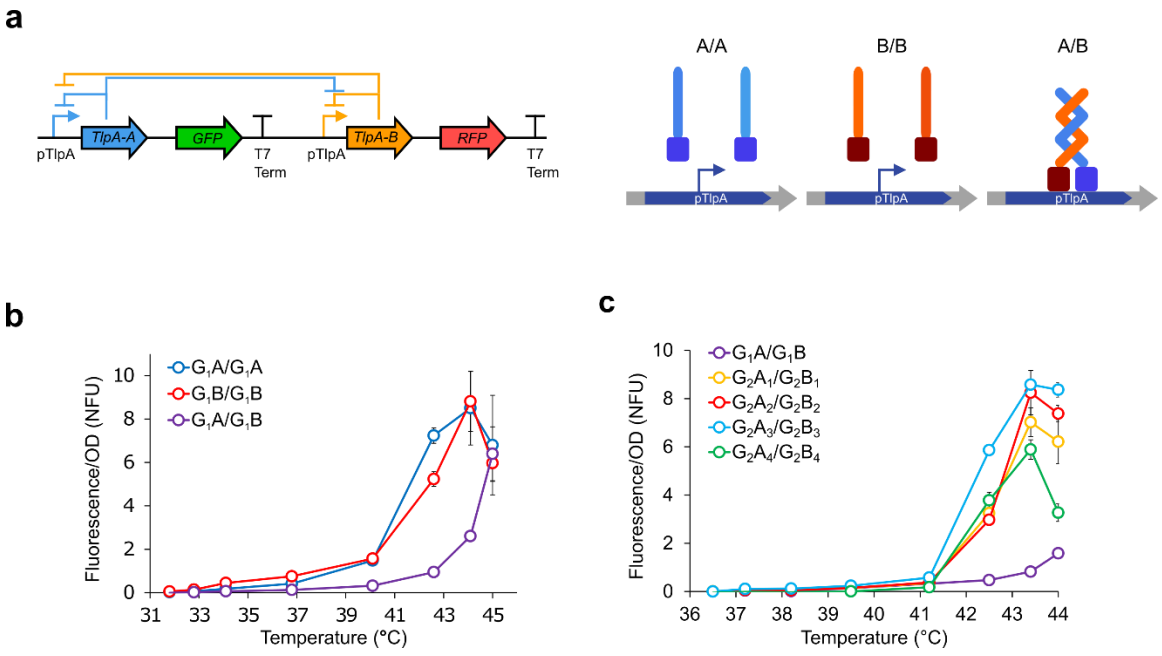

Figure 4-2: Evaluation of TlpA heterodimerization via reconstitution of promoter repression. **a**) Bacterial expression assay for heterodimerization preference. Left: diagram of bacterial genetic circuit containing two TlpA genes, each of which can encode one of the engineered variants. Bacteria harboring the G_1A/G_1A and G_1B/G_1B circuits can only produce the homodimeric coils, whereas the G_1A/G_1B circuits can produce either the homodimers or heterodimeric coils. Right: illustration of operator binding for engineered heterodimeric construct; only cells expressing both partners of the heterodimeric TlpA variant can repress the reporter gene at a certain temperature. **b**) OD-normalized fluorescence expression profile of *E. coli* harboring the plasmid constructs shown in **a**, with the single mutant G_1A and G_1B variants in the A and B positions, as a function of temperature (n = 3). Error bars represent ± s.e.m. NFU represents normalized fluorescent units. **c)** OD-normalized temperature-dependent fluorescence expression profiles of *E. coli* harboring plasmids bearing the four possible double mutant combinations of the G_1 variants and two additional candidate single mutations (n = 3). Only the heterodimeric pairings are shown. Error bars represent ± s.e.m.

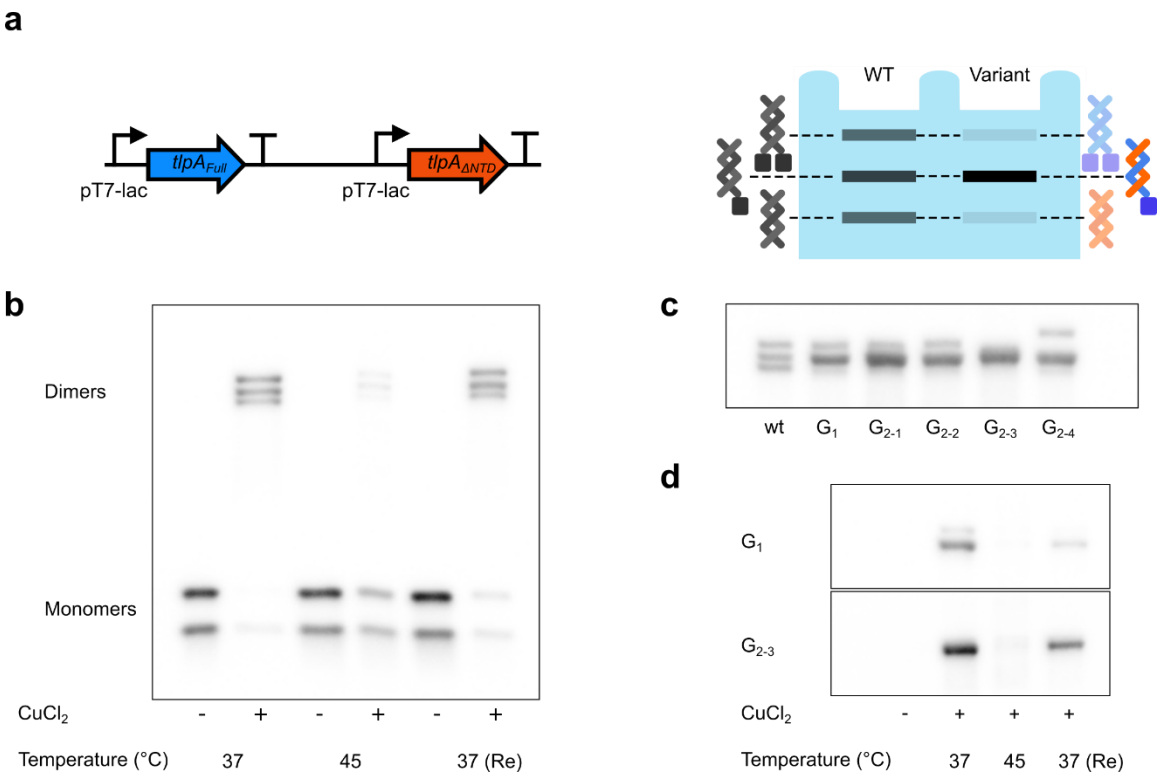

Figure 4-3: Validation of TlpA heterodimerization by electrophoresis. **a)** Left: diagram of genetic construct for simultaneous co-expression of engineered heterodimers of TlpA for biochemical assay. One open reading frame expresses the full length TlpA protein whereas the other ORF produces a truncated version missing its predicted N-terminal DNA-binding domain (ΔNTD). Each position can be occupied by any variant of TlpA, including the wild type protein and engineered mutants. Right: Diagram of the possible SDS-PAGE bands resulting from covalent crosslinking of the TlpA products expressed from this construct. The example in the left lane corresponds to the wild type homodimeric TlpA. The example in right lane corresponds to a pair of heterodimeric TlpA variants. **b)** Western blot of $CuCl_2$-catalyzed crosslinking reaction of wild-type TlpA in *E. coli* lysate followed by SDS-PAGE. Crosslinking was performed at 37 °C, at 45 °C, or at 37 °C to asses reannealing (Re) following a 10 minute incubation at 45 °C. Each condition is compared to a non-crosslinked control. The bottom bands on the gel show uncrosslinked monomers. **c)** $CuCl_2$ crosslinking, SDS-PAGE, and Western blot of the construct in **a** harboring wild type TlpA (wt), the first generation single mutant heterodimer (G_1), and the $G_{2\text{-}n}$ double mutant heterodimers. Crosslinking was performed at 37 °C. **d)** The thermal response of the G_1 and $G_{2\text{-}3}$ heterodimer constructs was analyzed in the absence and presence of $CuCl_2$ at 37 °C, 45 °C, or with 37 °C reannealing after 10 minute incubation at 45 °C.

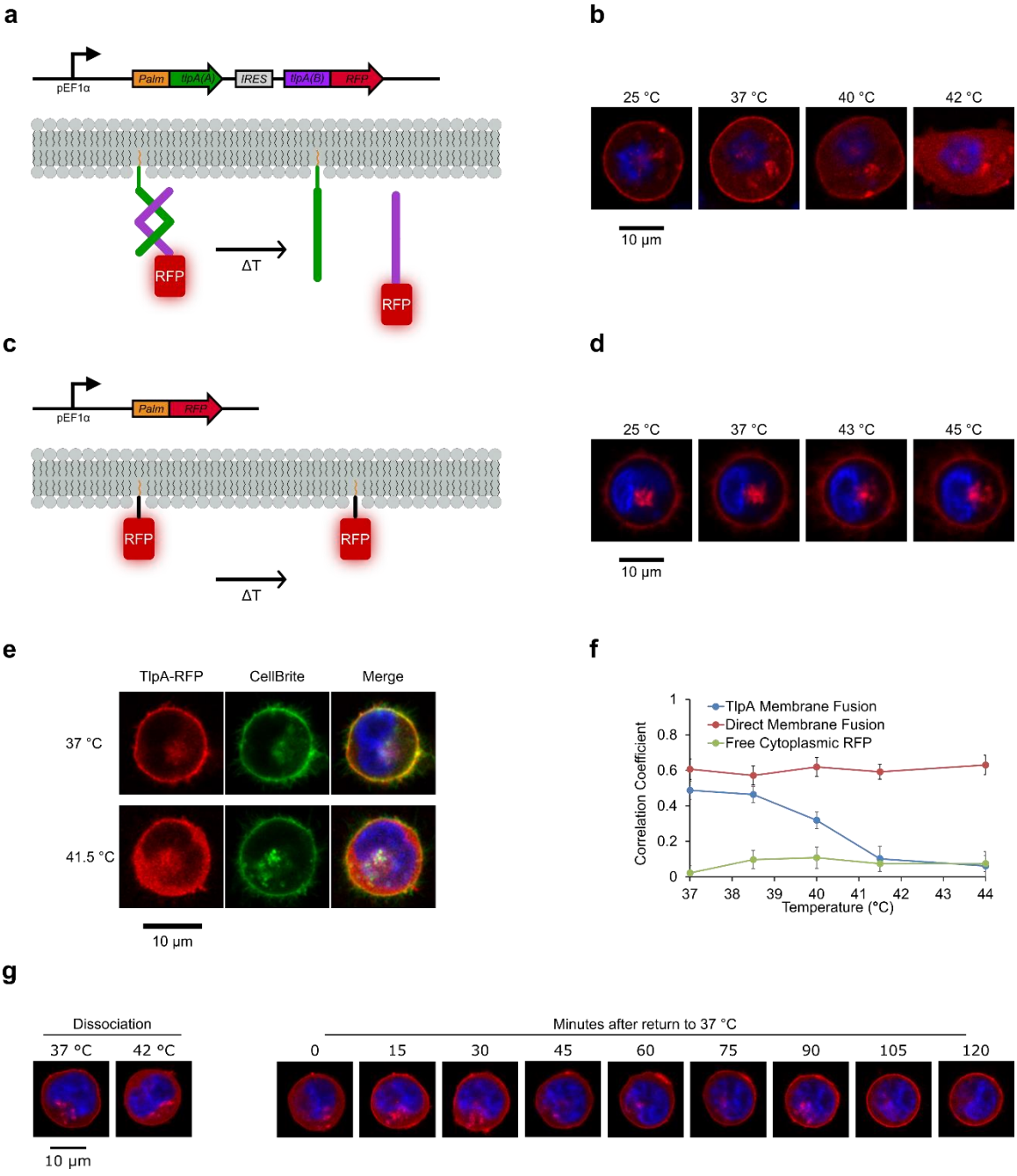

Figure 4-4: Membrane localization assay for TlpA activity in mammalian cells. a) Genetic construct (top) and schematic (bottom) for temperature-dependent localization of RFP at the plasma membrane. The $TlpA_{39}$-G_2A_3 strand is fused to a GAP43 palmitoylation motif, leading to its tethering to the lipid membrane. The partner $TlpA_{39}$-G_2B_3 strand is fused to RFP. At low temperature, the heterodimerization of these strands leads to RFP localization at the membrane. Upon heating, the RFP-fused strand dissociates from the membrane. **b**) Fluorescence images of a representative K562 cell transfected with the construct shown in **a**. Robust membrane localization of RFP fluorescence is observed at 25 °C and 37 °C. At 40 ºC, RFP begins to dissociate from the membrane, and by 42 °C red fluorescence is distributed throughout the cytoplasm. The nucleus is

stained in blue with Hoechst 33342 dye. **c**) Genetic construct (top) and experimental schematic (bottom) of directly palmitoylated RFP control. **d**) Fluorescence images of representative K562 cell transfected with the construct shown in **c,** displaying robust membrane localization throughout the temperature range tested. **e**) Representative fluorescence images of a K562 cell with a lentivirally delivered TlpA-mediated RFP localization construct (shown in **a**) and the membrane-staining dye CellBrite Fix 488. **f**) Pixel colocalization of RFP with the CellBrite 488 dye as a function of temperature in K562 cells stably expressing directly palmitoylated RFP (shown in **b**, n = 8), the TlpA-mediated membrane localization construct (shown in **a**, n = 15), and free cytosolic RFP (n = 8). Error bars represent ± s.e.m. **g**) Time series of fluorescent images of a representative K562 thermal reporter cell line before heating, after heating to 42 °C, and after re-equilibration to 37 °C. RFP re-accumulation at the plasma membrane was tracked in 15 minute intervals. Pixel intensity was normalized to the maximal per-image value.

4.7: Methods

Plasmid Construction and Molecular Biology

All plasmids were designed using the SnapGene software (GSL Biotech) and assembled via KLD mutagenesis or Gibson Assembly using enzymes from New England Biolabs. All plasmids and sequences will be deposited to Addgene. After assembly, constructs were transformed into NEB Turbo and NEB Stable *E. coli* (New England Biolabs) for growth and plasmid preparation. Constructs containing long homologous regions such, including all plasmids containing two TlpA ORFs, were propagated using NEB Stable. Thermal gene expression assays were performed in NEB Stable *E. coli*. Bacterial reporters of gene expression referred to in the text as GFP and RFP are mWasabi[1] and mCherry[2], respectively. The mammalian fusion protein fluorophore referred to in the text and figures as RFP is mScarlet-I[3]. TlpA, mCherry and mWasabi were obtained from our previous work[4]. mScarlet-I was obtained from AddGene (pmScarlet-i_C1, plasmid #85044). Coiled-coil structure prediction and helical wheel diagram annotation was performed using the software DrawCoil 1.0[5]. In the creation of dual-expression GFP/RFP thermal reporter plasmids such as that described in Fig. 1e, an additional terminator was placed upstream of each pTlpA promoter to suppress crosstalk from the weak upstream transcription previously observed from this element[4]. nhTlpA was designed using a homemade script to minimize codon homology while retaining protein sequence identity. Subsequently, 11 nucleotides were altered manually to minimize short repeats that prevented custom gene synthesis. The $nhTlpA_{39}$ gBlock was synthesized by Integrated DNA Technologies.

Bacterial Thermal Regulation Assay

Determination of temperature-dependent gene expression was performed as described previously[4]. Briefly, saturated precultures were diluted to OD_{600} = 0.1 and propagated at 30 °C until reaching OD_{600} = 0.3 as measured via Nanodrop 2000c (Thermo Scientific), at which point 25 uL aliquots were dispensed into PCR tubes with transparent caps (Bio-Rad) and incubated for 12 hours in a thermal gradient using a Bio-Rad C1000 Touch thermocycler. After thermal stimulus, fluorescence was measured using a Stratagene MX3005p qPCR (Agilent), after which cultures were diluted 4x, transferred into microplates (Costar black / clear bottom), and measured for OD_{600} using a Molecular Devices SpectraMax M5 plate reader. The background-corrected F/OD is reported as described previously[4].

Protein Expression and Purification for CD Spectroscopy

pET26b-based expression constructs were transformed into BL21-DE3 *E. coli* and grown on kanamycin-selective plates. Saturated overnight cultures were diluted 1 mL into 400 mL expression cultures and induced with a final IPTG (Sigma Aldrich) concentration of 1 mM at OD_{600} = 0.6. After 24 hours of expression at 25 °C, cultures were harvested by centrifugation using a JLA-16.250 rotor (Beckman Coulter) at 6,000 rpm and 4 °C for 8 minutes. Pellets were lysed using the detergent Solulyse in Tris Buffer (Genlantis) and debris was pelleted by centrifugation at 35,343 rcf in a JS-24.38 rotor (Beckman Coulter). Polyhistidine-tagged proteins were purified on an AKTA purifier (GE Healthcare) using 1 mL cOmplete columns (Roche) and buffer exchanged into 1x PBS (Corning) using Zeba spin desalting columns. Concentration was determined using the Pierce 660nm Protein Assay (Thermo Fisher Scientific) and proteins were stored at 4 °C until use. Proteins were subsequently analyzed within 24 hours of purification.

Circular Dichroism Spectroscopy

CD melting curves were taken using an Aviv Circular Dichroism Spectrophotometer (Model 60DS) at 222 nm with 0.1 minute equilibration time and 5 second averaging time. Purified proteins were diluted to 3 µM in 1x PBS and measured in a 1 mm quartz cuvette.

Temperature-dependent protein fluorescence measurement

Fluorescent proteins were purified as described above and diluted to 1 µM for analysis. 25 µL samples were placed in N=3 replicates in PCR strips with optically transparent caps (Bio Rad) into a Stratagene MX3005p qPCR (Agilent) for intensity mesaurements. Filter sets used for red, green, and blue proteins were ROX, FAM, and ATTO, respectively. Sample fluorescence was measured continuously as temperature was ramped from 25 °C to 50 °C in 1 °C increments and with 1 minute of equilibration time at each increment.

Mass-based validation of heterodimerization

Dual TlpA expression constructs were transformed into BL21-DE3 cells (NEB) and grown as 1 mL precultures in 2xYT/ampicillin for 20-24 hours at 30 °C in an Infors Multitron with shaking at 250 rpm. 10 µL saturated cultures were diluted into 4 mL 2xYT/ampicillin and returned to 30 °C. At OD_{600} – 0.6 to 0.7, cultures were induced with 4 µL of 1 M IPTG (Sigma Aldrich) and returned to 30 °C for 12 hours, at which point they were transferred into 2 mL centrifuge tubes (USA Scientific) and pelleted in a Beckman Microfuge 20 at maximum speed for 1 minute. Supernatant was carefully and completely aspirated with a pipette, and the pellet was weighed and frozen at -20 °C for at least 20 minutes. After

thawing, Solulyse in Tris Buffer (Genlantis) was added at 10 µL per 1 mg. Pellets were gently resuspended via pipetting and shaken in an Eppendorf ThermoMixer at room temperature (800 rpm for 20 minutes). Subsequently the tubes were spun at 13,000 rcf for 10 minutes and the lysate was diluted 5-fold in Solulyse in Tris Buffer. A pilot Western blot was performed and total TlpA band intensity was quantified for each variant, after which loading amounts for all variants were normalized to that of the wild type via dilution in Solulyse. For crosslinking, 1 µL of 50 mM $CuCl_2$ (Sigma Aldrich) was added to 10 µL lysate in an Eppendorf microcentrifuge tube. The lysate and $CuCl_2$ solution were pre-heated separately for 5 minutes prior to co-incubation. Subsequently, the lysate and crosslinker mixture was shaken at 800 rpm for 10 minutes in an Eppendorf ThermoMixer at the desired temperature. After 10 minutes of $CuCl_2$-catalyzed crosslinking, the reaction was quenched with 11 µL Laemmli buffer (Bio Rad). For uncrosslinked samples, 10 uL Laemmli buffer was added to the lysate at the appropriate temperature. SDS-PAGEwas performed using 7.5% pre-cast polyacrylamide gels (Bio Rad) run at 75 V for 140 minutes. Western blotting was performed using the Transblot Turbo apparatus and nitrocellulose membrane kit (Bio Rad). Transfer was performed at 25 V for 7 minutes. Membranes were blocked with 5% w/v Blotto milk (Santa Cruz Biotechnology) in 0.05% TBS-Tween for 1 hour at room temperature. Primary staining was performed using the mouse anti-HA sc-7392 antibody (Santa Cruz Biotech) overnight at 4 °C. Blots were then washed three times for 15 minutes at 4 °C with 0.05% TBS-Tween and stained for 4 hours with goat anti-mouse IgG-HRP sc-2005 (Santa Cruz Biotech) at room temperature. After three 15-minute washes, HRP visualization was performed using Supersignal West Pico PLUS reagent (Thermo Fisher Scientific). Imaging was performed in a Bio-Rad ChemiDoc MP gel imager.

Mammalian cell culture

K562 cells (gift of D. Baltimore) were cultured in RPMI 1640 media (Thermo Fisher Scientific) with 1x Penicillin/Streptomycin (Corning). Transient transfection was performed using Lonza 4D nucleofection with SF Cell Line buffer and the pre-programmed K562 protocol. Lentivirus was prepared using a third-generation viral vector and helper plasmids (gifts of D. Baltimore). Virus was packaged in HEK293T cells grown in 10 cm dishes after 2 days of transfection and concentrated via the Lenti-X reagent (Takara Bio). Infection was performed by resuspending viral pellets in 250 uL RPMI and spinfecting 1E6 K562 cells in 1 mL RPMI with 10 µL virus at 800 xg, 30 °C, for 90 minutes. Experiments were performed at least five passages after infection.

Live cell microscopy

Delta-T dishes (Bioptechs) were coated with 400 µL 0.1 mg/mL Poly-D Lysine (Sigma Aldrich) for 30 minutes. Meanwhile, 1E6 K562 cells were pelleted at 300 rcf for 5 minutes and resuspended in staining solution (1x PBS or HBSS with 2.5 µg/mL Hoechst 33342, Thermo Fisher Scientific). For Golgi staining, the solution (in HBSS) also contained BODIPY FL C_5-Ceramide complexed to BSA (Thermo Fisher Scientific, 50 nM final concentration). Cells were stained at room temperature for 10 minutes before being pelleted and resuspended in 1 mL RPMI 1640. For co-localization experiments, the staining solution (in HBSS) also contained CellBrite Fix 488 at 1x concentration as described in the product manual, and staining was performed at 37 °C for 10 minutes. After at least 20 minutes of coating, PDL was aspirated from the Delta-T dishes, which were then rinsed once with 1x

PBS and dried. Cells were then transferred to the Delta-T dishes, which where adhesively affixed to the swinging plates of an Allegra X-12 centrifuge with SX4750 rotor (Beckman Coulter) and centrifugated at 30 °C for 15 minutes at 300 rcf. Imaging was performed at the California Institute of Technology confocal microscopy facility using an LSM880 (Zeiss) with Airyscan. Cells with sufficient overall brightness to discern membrane contrast were imaged; the membrane localization of dimmer cells could not be discerned in our thermal imaging configuration but was observable under higher magnification on a conventional glass slide (**Supplementary Fig. 4-S14**). Delta-T dishes were mounted onto the thermal stage interfaced with a Bioptechs Delta T4 Culture Dish Controller and imaged using a 1080-378 C-Achroplan 40x/0.80 W objective. Airyscan processing was performed in 2D mode using default settings.

Image analysis

Image analysis was performed using the Zeiss Zen Black software for pre-processing and CellProfiler[6] for correlation quantification. Images were manually cropped to include only a single cell per ROI, with approximately 408x408 pixel FOVs. For cells with poor attachment to the plate, resulting in position offsets between the red, blue, and green channels, frame alignment between the red and green channels was performed in Zen Black. All available transformations were sampled and the best-aligned transformation on a per-cell basis was used. Blue channel alignment was performed in CellProfiler using the Mutual Information module, correlating the blue channel image with the inverted red channel image. Exported images were then loaded in CellProfiler and analyzed using a custom pipeline (**Supplementary File 4-F1)**. Briefly, cell boundaries were determined from red channel

using Hoescht 33342-stained nuclei as primary seed objects. Atypically bright green clusters frequently observed on the green channel were excluded from quantification, as were the Golgi-associated TlpA clusters on the red channel. Colocalization was calculated for the ROI defined between the outer cell membrane and the nucleus. The nucleus was excluded because it acts as a diffusion barrier to TlpA-RFP but not to free mScarlet-I. For the free mScarlet-I cell line in **Fig. 4-4f**, a modified pipeline using the CellBrite Fix 488 stain for cell boundary determination was used to improve the detection of cell edges (**Supplementary File 4-F2**). For the Direct Membrane Fusion data set in **Fig. 4-4f**, the 44 °C point was acquired in a separate experiment using the same cell line and is consistent with the 43 °C and 45 °C data points of the original data set (**Supplementary Fig. 4-S15**).

4.8: Supplementary Figures

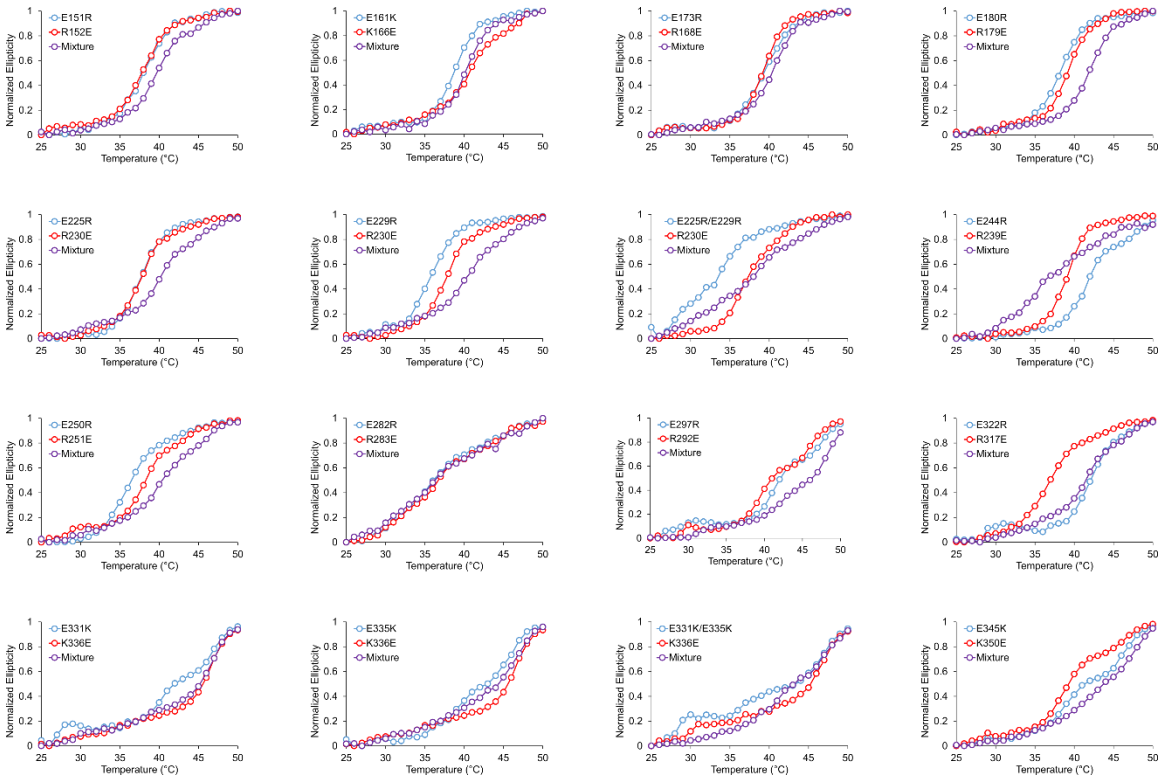

Supplementary Figure 4-S1: Circular dichroism melting curves of engineered TlpA variants. Coiled-coil fragments corresponding to residues 69-359 of TlpA were purified from *E. coli* and assayed via CD spectroscopy. Monitoring the ellipticity at 222 nm, corresponding the prototypical peak of the α-helical spectrum, enables tracking the conformation of TlpA as it transitions from the dimeric coiled-coil state to a monomeric random coil configuration.

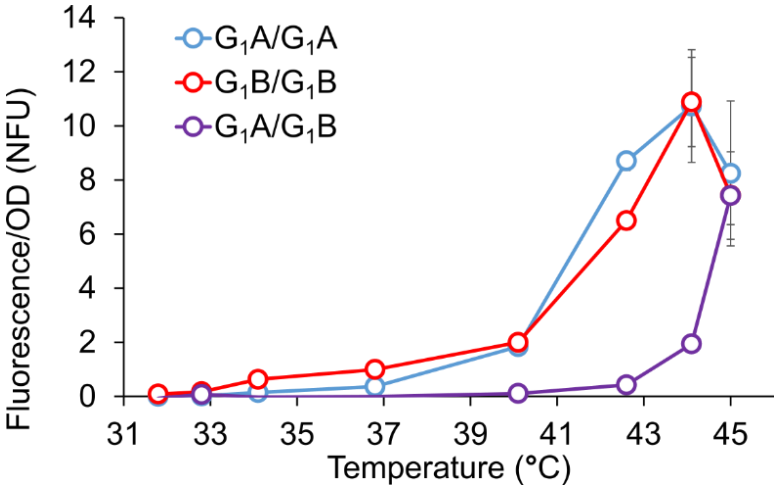

Supplementary Figure 4-S2: Thermal RFP expression profiles of the constructs shown in **Fig. 4-2b** (n = 3). Error bars represent ± s.e.m.

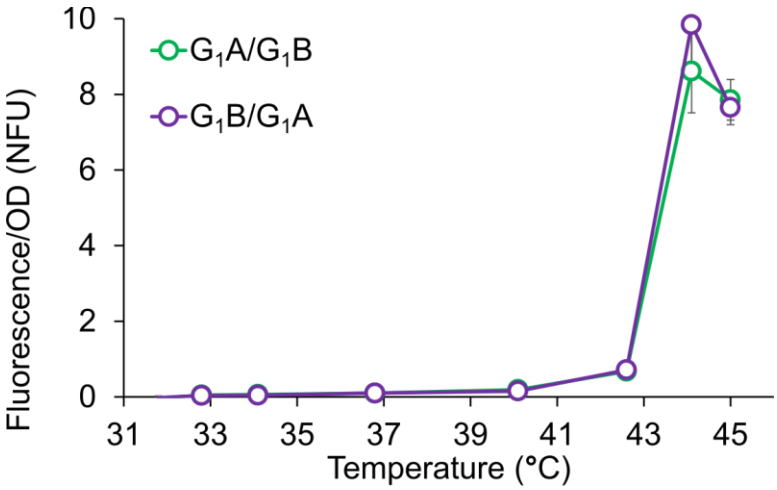

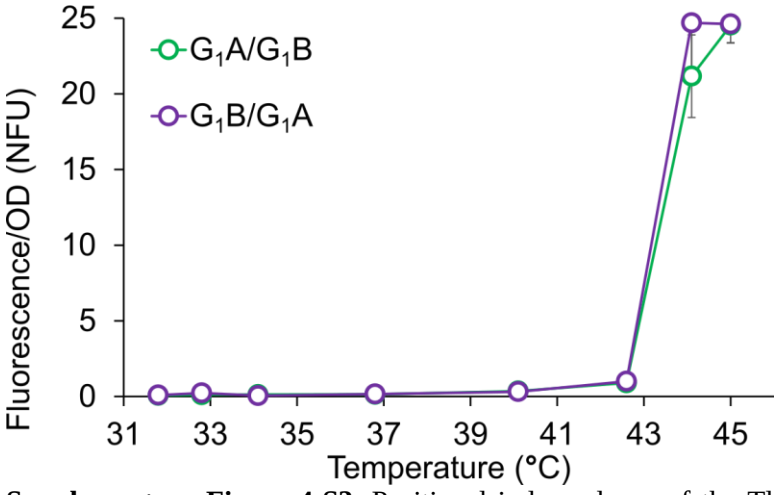

Supplementary Figure 4-S3: Positional independence of the TlpA co-expression construct. The positions of TlpA-G_1A and TlpA-G_1B within the heterodimer co-expression construct in **Fig. 4-2b** were exchanged and the thermal GFP (top) and RFP (bottom) expression profile was determined (n = 4). No significant differences were observed in the gene expression profile, thereby excluding position-dependent effects on TlpA behavior within the circuit. Error bars represent ± s.e.m.

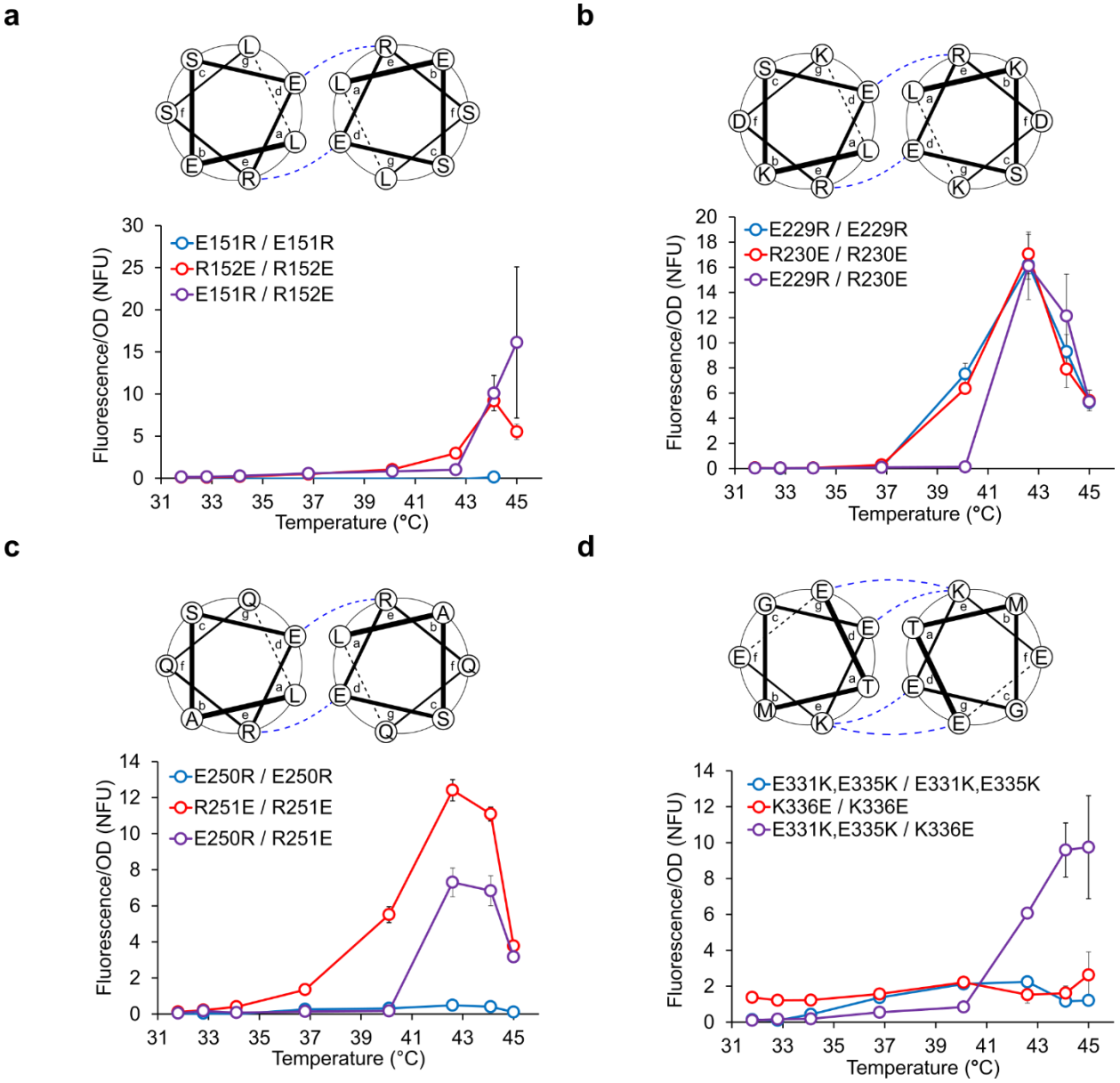

Supplementary Figure 4-S4: Screening of rationally designed mutant panel via bacterial thermal gene expression assay. Four positions in the TlpA coiled-coil were selected for mutagenesis based on the predicted similarity of their ionic interaction pattern to the G_1A/G_1B mutant pair according to the heptad repeat register prediction of Koski *et al*. The following mutations were examined: **a)** E151R and R152E **b)** E229R and R230E, **c)** E250R and R251E, and **d)** E331K/E335K and K336E. The predicted interaction pattern of the wild type protein is depicted (top), and the thermal GFP expression profile is reported (bottom). N = 3. The E229R/R230E and E250R/R251E pairs were selected for introduction into the TlpA-G_1A and G_1B variants. Error bars represent ± s.e.m.

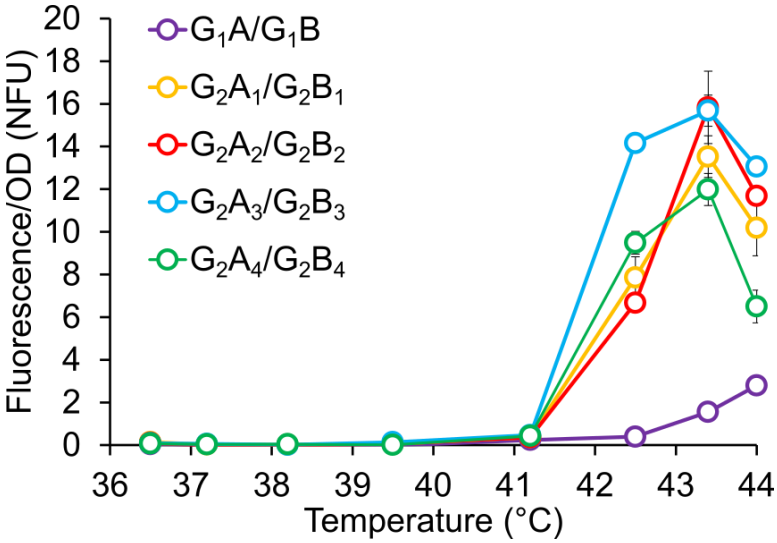

Supplementary Figure 4-S5: Thermal RFP expression profiles of the first and second-generation heterodimers shown in **Fig. 4-2c** (n = 3). Only the construct containing one copy of each heterodimeric strands are depicted because the X_nA/X_nB homodimeric construct were unable to propagate without accumulating deletion mutations in the TlpA promoters or fluorescent protein open reading frames. Error bars represent ± s.e.m.

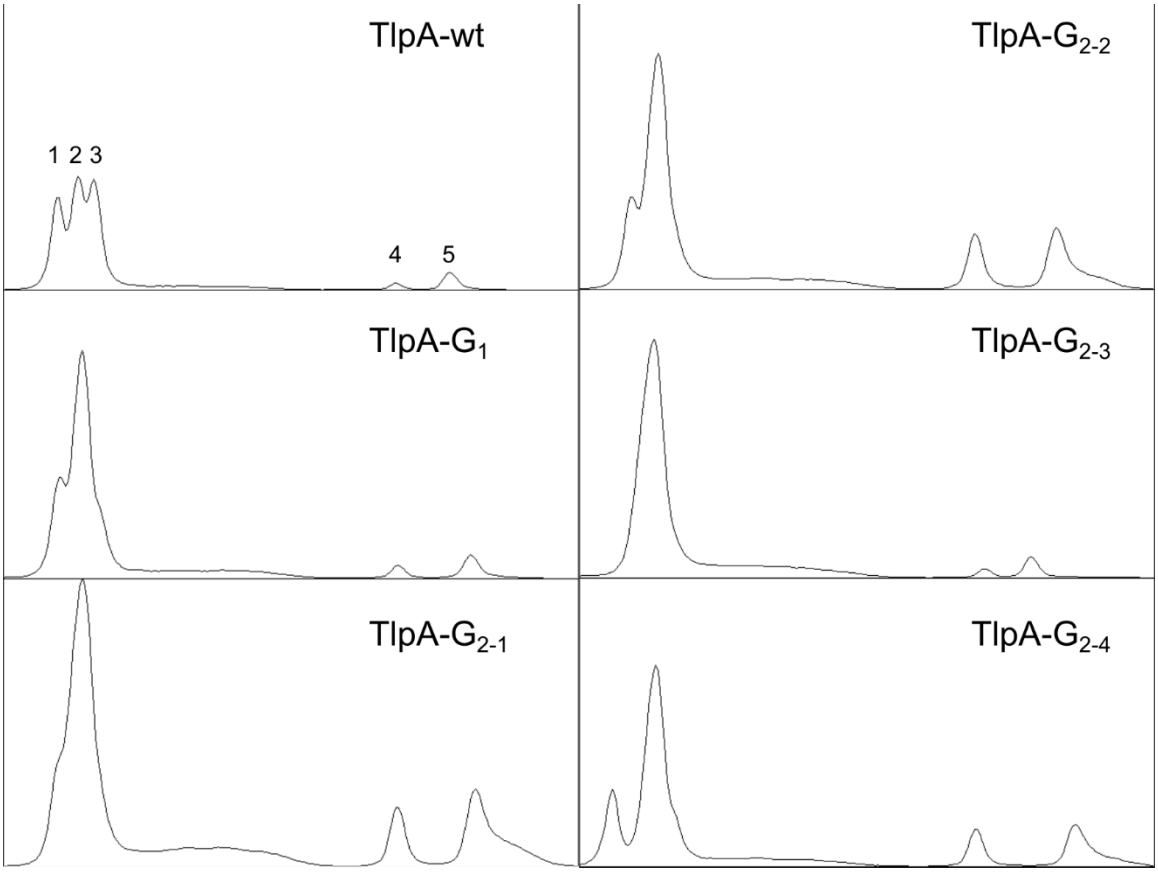

Supplementary Figure 4-S6: Western blot band intensity profiles of co-expressed full and truncated TlpA strands in **Fig. 4-3c**. Note that samples lacking a distinct band corresponding to the truncated homodimer (3), such as TlpA-G_1, nevertheless display higher band intensity for the truncated uncrosslinked strand (5) relative to the full-length uncrosslinked species (4), confirming that the lack of a low molecular weight homodimer at position 3 results from reduced homodimer affinity rather than full depletion of the light TlpA strand by heterodimer pairing. This is consistent with cationic and anionic TlpA variants having different homodimerization affinities at 37 °C.

a

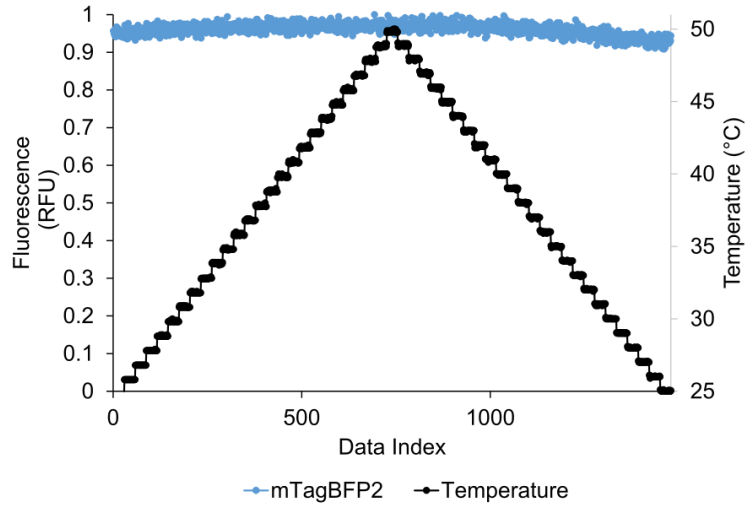
Fluorescence (RFU)
Temperature (°C)
Data Index
mTagBFP2
Temperature

b

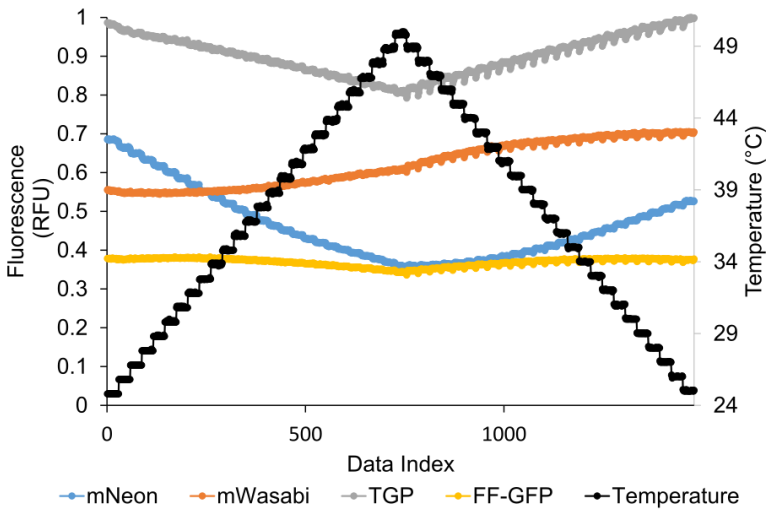
Fluorescence (RFU)
Temperature (°C)
Data Index
mNeon
mWasabi
TGP
FF-GFP
Temperature

c

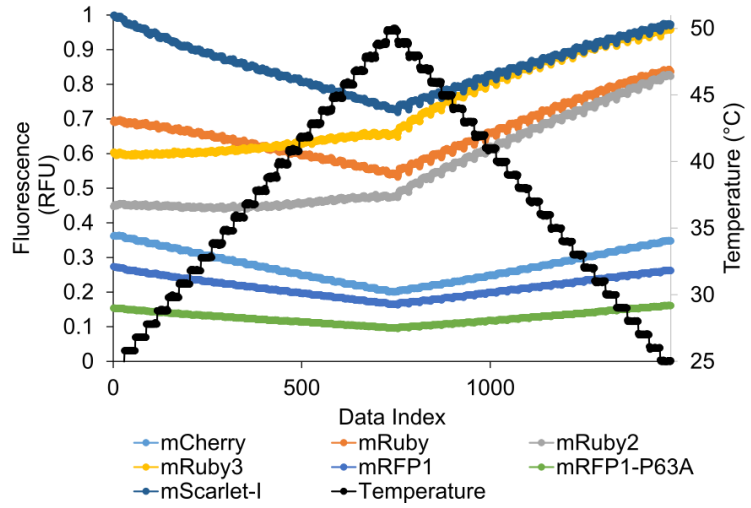
Fluorescence (RFU)
Temperature (°C)
Data Index
mCherry
mRuby
mRuby2
mRuby3
mRFP1
mRFP1-P63A
mScarlet-I
Temperature

Supplementary Figure 4-S7: Thermal stability of a panel of blue (**a**), green (**b**), and red (**c**) fluorescent proteins. Proteins were prepared in equimolar concentrations and their fluorescence was measured in an rtPCR thermocycler upon a thermal ramp from 25 °C to 50 °C and subsequent re-annealing to 25 °C, with readings taken continuously over 1 minute intervals. Signal intensity is normalized to the maximum for each given experiment. Because different filter sets were used for the three classes of proteins, relative brightness does not correlate between the red, green, and blue channels. While some proteins such as FF-GFP demonstrated more stable signal over the temperature range tested, the overall brightness was maximal in mScarlet-I and TGP. However, TGP demonstrated significant aggregation when expressed as an untagged cytosolic protein in mammalian cells so mScarlet-I was chosen as the reporter for subsequent experiments.

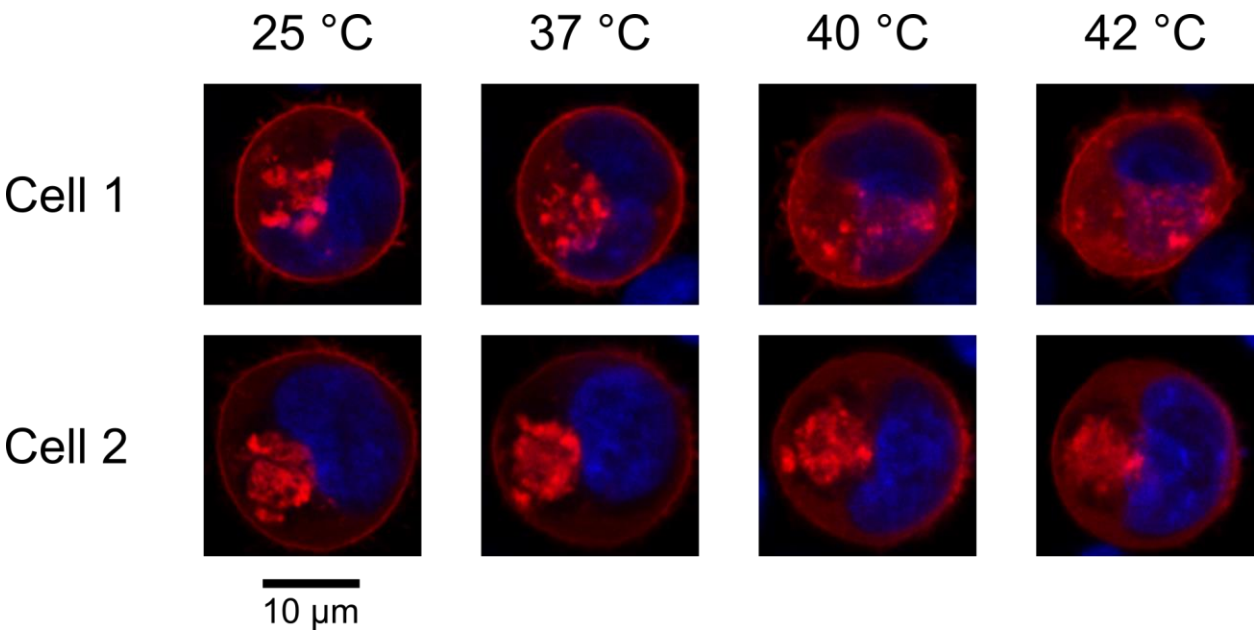

Supplementary Figure 4-S8: Additional replicates for TlpA membrane localization experiment in **Figure 4-4b**. Pixel intensity was normalized to the maximal per-image value.

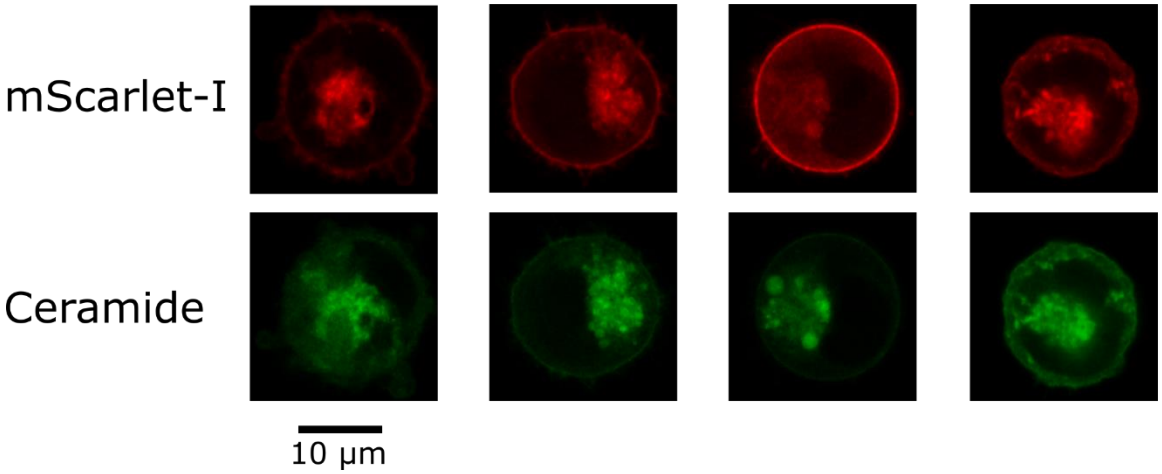

Supplementary Figure 4-S9: K562 cells transfected with the construct shown in **Fig. 4-4a** were stained with BODIPY-C5-Ceramide to label the Golgi transport pathway. Staining morphology was similar to the localization of the mScarlet-I TlpA cargo protein. Four representative cells are shown. Pixel intensity was normalized to the maximal per-image value.

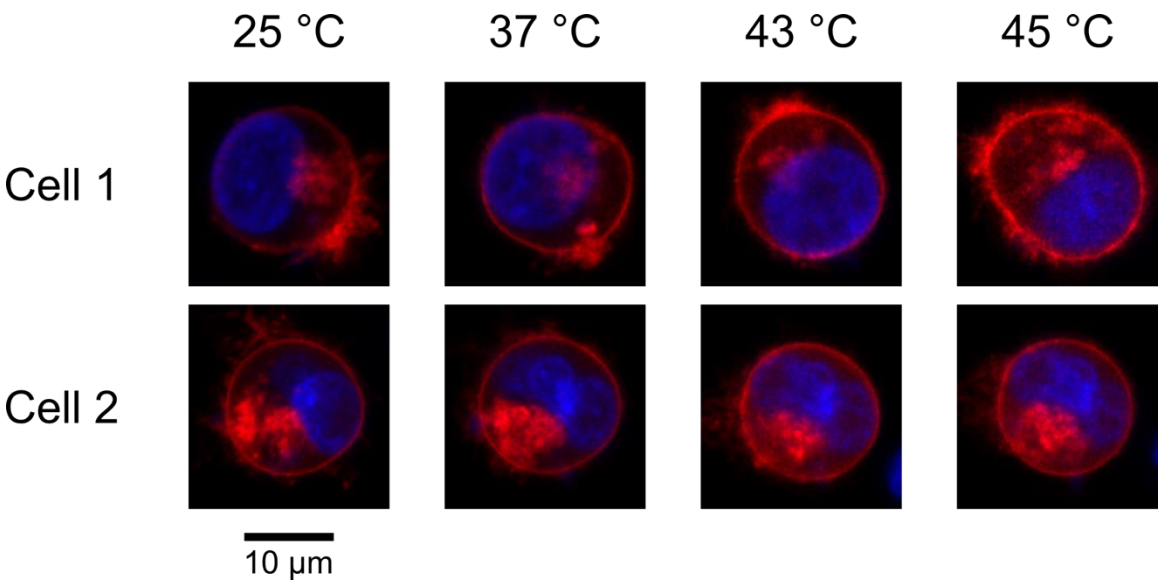

Supplementary Figure 4-S10: Additional replicates of K562 cells transfected with a construct bearing directly palmitoylated mScarlet-I, as in **Fig. 4-4d**. Robust membrane localization was observed up to 45 °C in most cells. Data presented are representative of two separate experiments. Pixel intensity was normalized to the maximal per-image value.

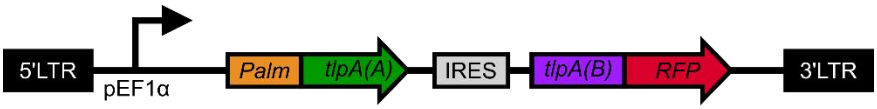
5'LTR
pEF1α
Palm
tlpA(A)
IRES
tlpA(B)
RFP
3'LTR

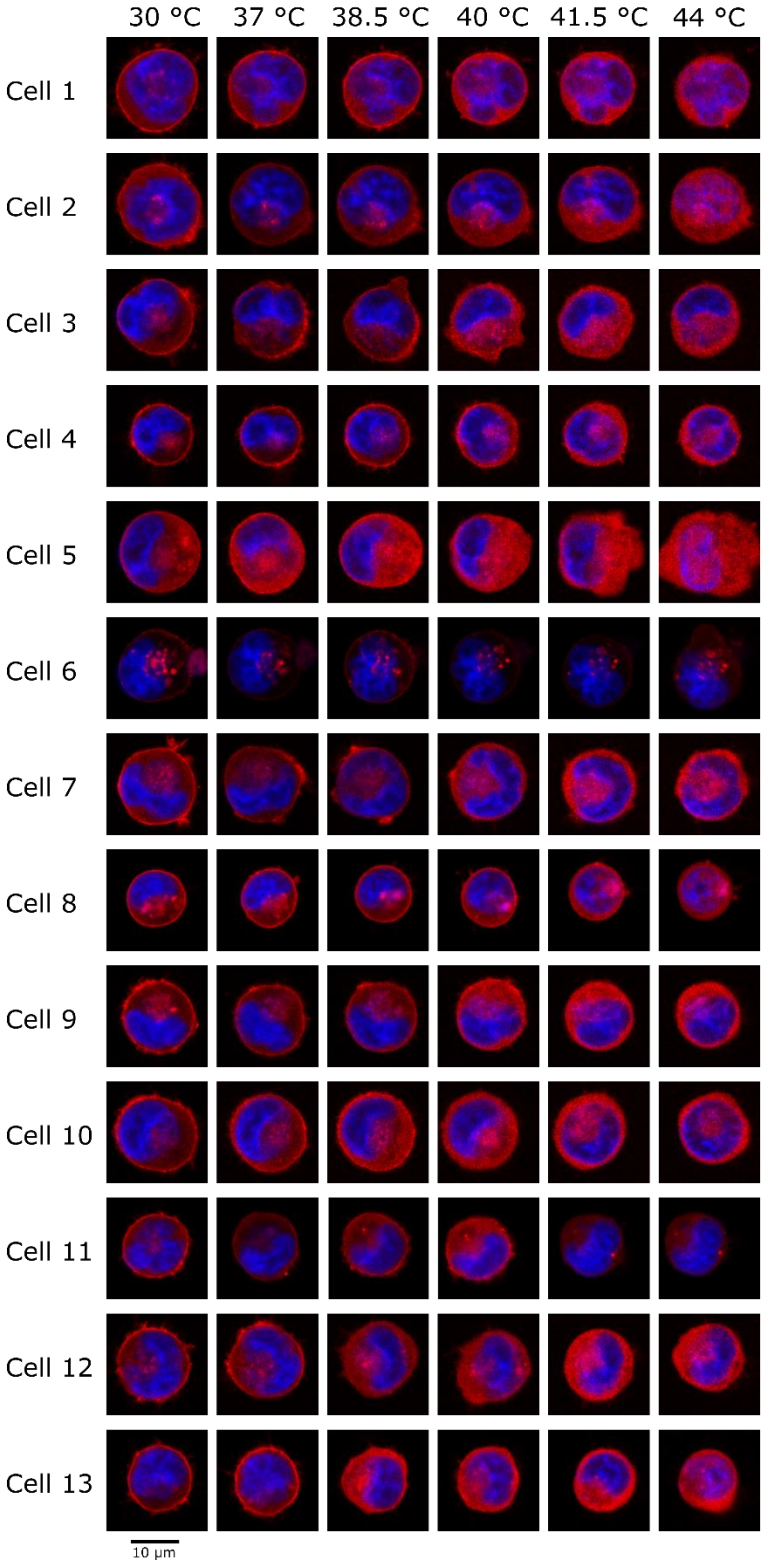
30 °C
37 °C
38.5 °C
40 °C
41.5 °C
44 °C
Cell 1
Cell 2
Cell 3
Cell 4
Cell 5
Cell 6
Cell 7
Cell 8
Cell 9
Cell 10
Cell 11
Cell 12
Cell 13
10 µm

Supplementary Figure 4-S11: Top: Lentiviral construct for membrane-localized RFP delivery containing nonhomologous $TlpA_{39}$-G_2A_3. Bottom: Fluorescence images at different temperatures of K562 cells lentivirally transduced with the nonhomologous TlpA-mediated membrane localization system. Pixel intensity was normalized to the maximal per-image value.

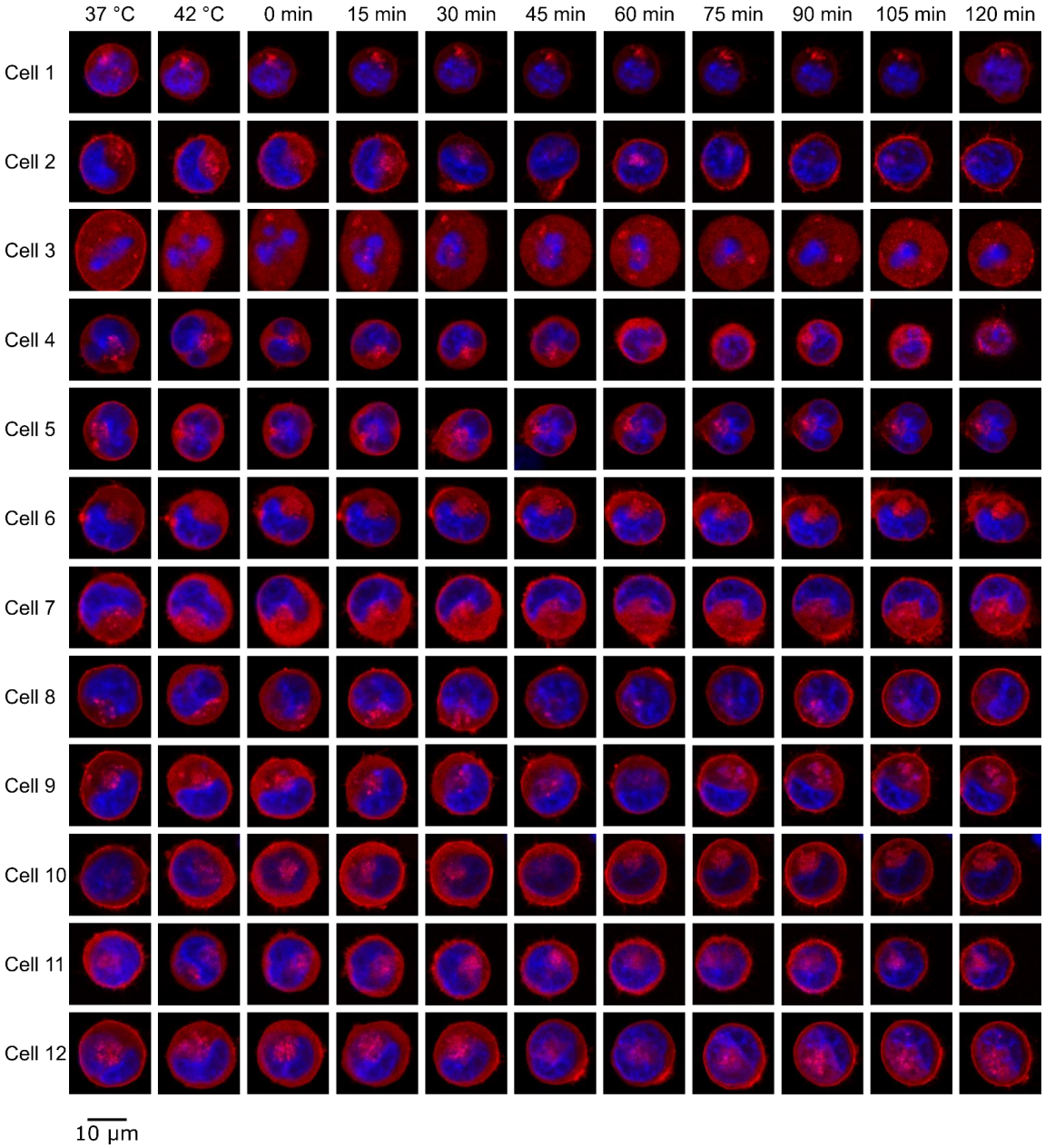

Supplementary Figure 4-S12: Replicates of the membrane delocalization reversibility assay shown in **Fig. 4-4g**. Pixel intensity was normalized to the maximal per-image value.

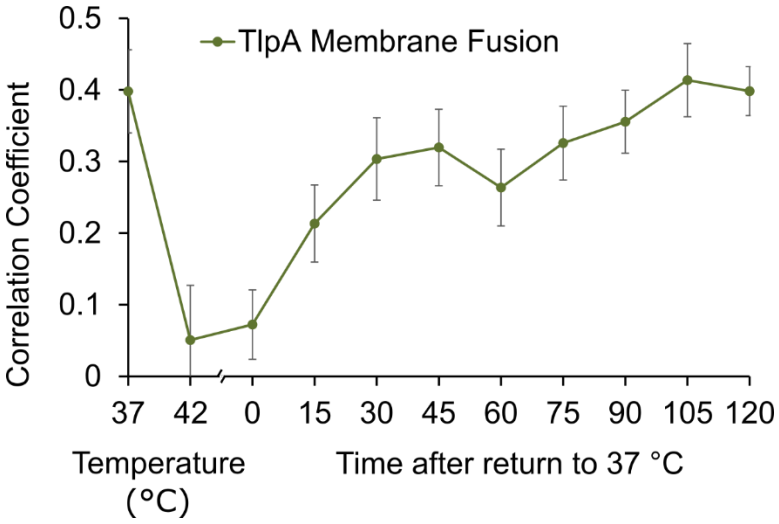

Supplementary Figure 4-S13: Reversibility of TlpA association in mammalian cells. K562 cells transduced with the lentiviral construct carrying the TlpA-mediated RFP membrane associated construct were assayed by confocal microscopy. Cells were imaged at 37 ℃, elevated to 42 ℃ for 5 minutes, and returned to 37 ℃, at which point they were imaged every 15 minutes. Error bars represent ± s.e.m.

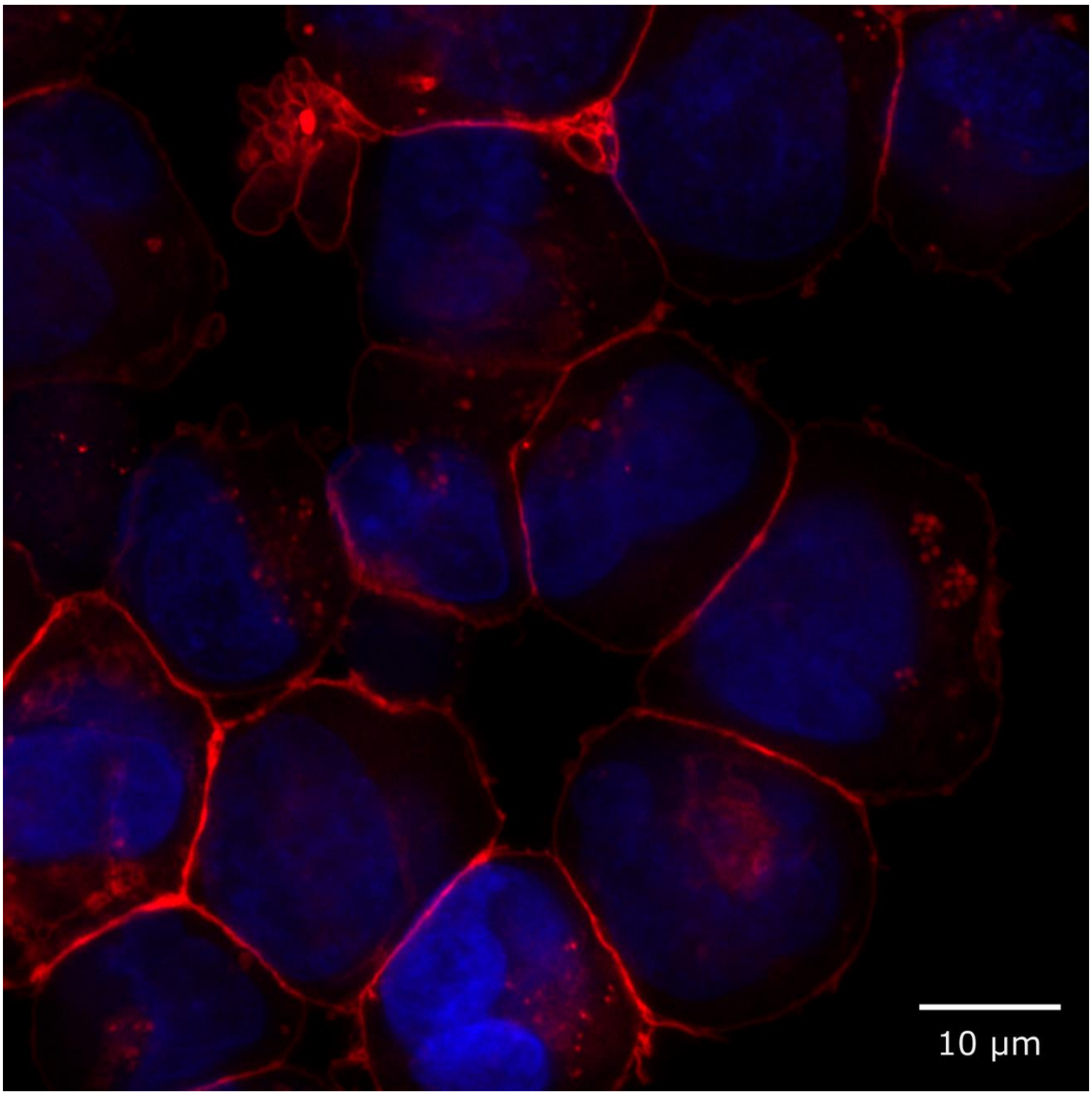

Supplementary Figure 4-S14: Confocal imaging of K562 cell line transduced with the lentiviral construct depicted in **Supplementary Figure 4-S11**. Cells were pelleted, deposited on a glass slide, sealed with a cover slip, and imaged on an LSM880 with a Plan-Apochromat 63x/1.4 Oil DIC M27 objective with oil immersion. Note that all cells, regardless of local cytoplasmic or membrane brightness, display visible RFP accumulation along the plasma membrane.

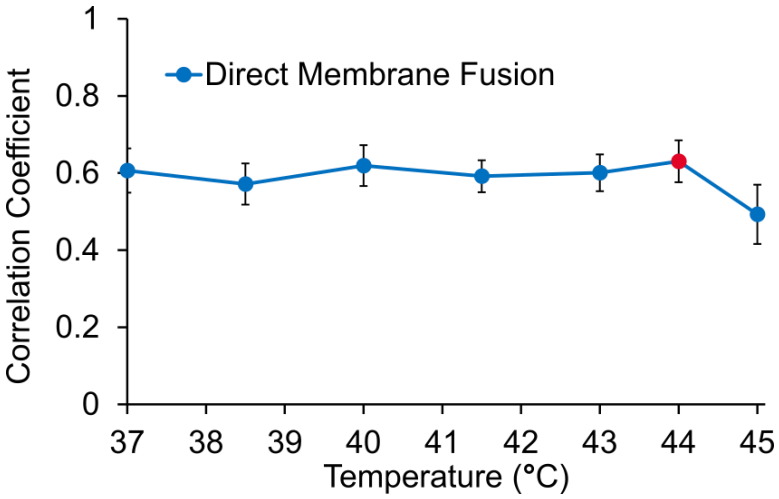

Supplementary Figure 4-S15: CellProfiler quantification of the two data sets contributing to the Direct Membrane Fusion curve in **Fig. 4-4f**. The data point acquired separately at 44 °C is highlighted in red.

Supplementary Table 4-T1: Second-generation TlpA mutants utilized in this study.

G_2A_1	E180R + E229R
G_2B_1	R179E + R230E
G_2A_2	E180R + R230E
G_2B_2	R179E + E229R
G_2A_3	E180R + E250R
G_2B_3	R179E + R251E
G_2A_4	E180R + R251E
G_2B_4	R179E + E250R

4.9: Supplementary References

(1) Ai, H.; Olenych, S. G.; Wong, P.; Davidson, M. W.; Campbell, R. E. Hue-Shifted Monomeric Variants of Clavularia Cyan Fluorescent Protein: Identification of the Molecular Determinants of Color and Applications in Fluorescence Imaging. *BMC Biol.* **2008**, *6*, 13. https://doi.org/10.1186/1741-7007-6-13.

(2) Shaner, N. C.; Campbell, R. E.; Steinbach, P. A.; Giepmans, B. N. G.; Palmer, A. E.; Tsien, R. Y. Improved Monomeric Red, Orange and Yellow Fluorescent Proteins Derived from Discosoma Sp. Red Fluorescent Protein. *Nat. Biotechnol.* **2004**, *22* (12), 1567–1572. https://doi.org/10.1038/nbt1037.

(3) Mastop, M.; Bindels, D. S.; Shaner, N. C.; Postma, M.; Gadella, T. W. J.; Goedhart, J. Characterization of a Spectrally Diverse Set of Fluorescent Proteins as FRET Acceptors for MTurquoise2. *Sci. Rep.* **2017**, *7* (1), 11999. https://doi.org/10.1038/s41598-017-12212-x.

(4) Piraner, D. I.; Abedi, M. H.; Moser, B. A.; Lee-Gosselin, A.; Shapiro, M. G. Tunable Thermal Bioswitches for in Vivo Control of Microbial Therapeutics. *Nat. Chem. Biol.* **2017**, *13* (1), 75–80. https://doi.org/10.1038/nchembio.2233.

(5) Grigoryan, G.; Keating, A. Structural Specificity in Coiled-Coil Interactions. *Curr. Opin. Struct. Biol.* **2008**, *18* (4), 477–483. https://doi.org/10.1016/j.sbi.2008.04.008.Structural.

(6) Carpenter, A. E.; Jones, T. R.; Lamprecht, M. R.; Clarke, C.; Kang, I. H.; Friman, O.; Guertin, D. A.; Chang, J. H.; Lindquist, R. A.; Moffat, J.; et al. CellProfiler: Image Analysis Software for Identifying and Quantifying Cell Phenotypes. *Genome Biol.* **2006**, *7* (10). https://doi.org/10.1186/gb-2006-7-10-r100.